Remarkable response of hollow thermoplastic microspheres-elastomer matrix composites in uniaxial tension

Coret M.[1], Verron E.[1], Rublon P.[2], and Leblé B.[2]

[1]Nantes Université, Ecole Centrale Nantes, CNRS, GeM, UMR 6183, 1 rue de la Noë, Nantes, 44321, France

[2]Naval Group Research, Technocampus Océan, rue de l' Halbranne, 44340, Bouguenais, France

May 9, 2022

Abstract

In the last few years, the mechanical response of hollow thermoplastic microspheres-elastomer matrix composites has been investigated. The large majority of the studies focuses on their compressive properties and particularly on the stress-strain response. In the present paper, large strain uniaxial tension experiments are conducted on thermoplastic microspheres filled polyurethane elastomer. Six volume fractions of microspheres are considered. Thanks to a two-camera setup and digital image correlation measurements, the volumetric response of the materials is extensively analyzed. As a major result, the remarkable volumetric behaviour is highlighted: the hydrostatic pressure vs. volume change curves admit several extrema that may be read as the macroscopic signature of the complex microstructural phenomena involved during deformation. Moreover, it is shown that the size of the volumetric loading-unloading hysteresis loop is directly related to the volume fraction of microspheres in the materials.

1 Introduction

Polymer syntactic foams, i.e. materials made of microspherical inclusions embedded in a matrix, are employed in various applications for their buoyant and/or acoustic behaviours, their compressive strength but also their thermal insulation properties (Gupta et al, 2014). In most of cases, glass microspheres are considered in rigid thermoset resins (Gupta et al, 2010) or elastomer (Brown et al, 2018) matrices.

For the last few years, new thermoplastics microballoons/elastomer matrix composites have been developed. They are made of hollow thermoplastics microspheres (HTMs in the following, commercial name Expancel) encapsulating a gas (Curd et al, 2021) that act as fillers in silicone (Shorter, 2014) or polyurethane (Yousaf et al, 2020) elastomer matrix. In a large majority of studies devoted to these materials, the focus is laid on their compressive properties: such experimental results are proposed by Paget et al (2021); Yousaf et al (2020); Smith et al (2021). These investigations being very recent, only few attempts of modelling have been published; roughly speaking authors are trying to account for the (reversible) buckling of the HTMs by different approaches: simple physical models (De Pascalis et al, 2013), numerical or analytical homogenization techniques (Shrimali et al, 2020), or phenomenological compressible constitutive equations (Smith et al, 2021).

For uniaxial tension, and to the best of our knowledge, only two studies report experiments on dumbbell samples:

- Shorter et al (2007) present the loading curves of an unfilled and three HTMs filled silicone elastomers. It is shown that for low strain, higher the microspheres content, higher the stiffness; the inverse phenomenon is observed for large strain ($> 175\%$ strain).

- Yousaf et al (2022) propose a thorough investigation of the cyclic response of HTMs/polyurethane elastomer syntactic foams up to 50% strain. Among the results, it is shown that the presence of microballoons highly increases the size of the loading-unloading stress-strain hysteresis loop.

These two studies focus on macroscopic stress-strain unidimensional response but do not investigate the compressibility of these materials, even if this property is of major importance in applications.

In the following, the uniaxial tensile response of HTMs filled polyurethane elastomer is reported. Experimental methods are presented in the next section: materials and samples, then the two-camera setup are described. Results are presented and discussed in Section 3. First, the data treatment is detailed. Then, after the presentation of classical stress-strain results, the focus is laid on the volumetric response of the materials: hydrostatic pressure vs. volume change curves are drawn and their comprehensive analysis is proposed. Finally, a short conclusion closes the paper.

2 Methods

2.1 Materials and samples

Materials are made of a polyurethane elastomer matrix filled with HTMs. Six volume fractions of HTMs (which will be sometimes referred to as "porosity" in the following) are considered: 0, 5, 10, 15, 20, and 25% (nominal data given by the supplier). The

volume fraction of each specimen has been verified with the following method. First, the density of the polyurethane matrix is considered independent of the HTMs volume fraction: it is equal to the one of the 0% material. Second, samples being produced by a cutting punch, their in-plane geometry is assumed well-established. The thickness of specimen is measured by a caliper with a precision of $\pm$ 0.01 mm, and the weight by a balance with a precision of $\pm$ 0.002 g. Then the actual porosities are calculated. The corresponding results are given in Table 1, each of them corresponds to the mean value of three measurements on three different samples. In the following, the actual values will

Nominal porosity (%)	5	10	15	20	25
Actual porosity (%)	4.6 ± 0.10	9.3 ± 0.33	13.5 ± 0.18	17.5 ± 0.14	23.2 ± 0.18

Table 1: Nominal and actual volume fractions of HTMs in the five filled materials.

be considered for the computations, but for the sake of simplicity the nominal ones will be used in the presentation of the results.

The geometry of the dumbbell samples are shown in Figure 1(left). Fig. 1(right)

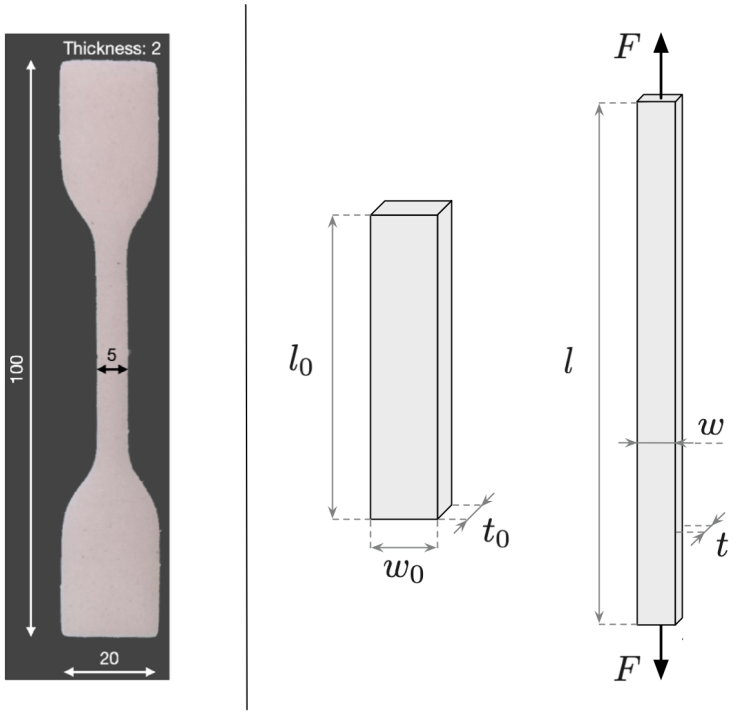

Figure 1: Sample. Left: dimensions (mm). Right: notations.

sketches the uniaxial tensile test, and introduces the notations: $l_0 \times w_0 \times t_0$ strain gauge deforms into $l \times w \times t$ with the force F. Practically, l_0 is about 20-25 mm. Thus, we define

- the three stretch ratios

$$\lambda = \frac{l}{l_0} \ , \ \lambda_w = \frac{w}{w_0} \ , \ \lambda_t = \frac{t}{t_0}, \tag{1}$$

respectively in the longitudinal, width, and thickness directions,

- and the nominal (first Piola-Kirchhoff) and true (Cauchy) stresses:

$$P = \frac{F}{w_0 \times t_0} \ , \ \sigma = \frac{F}{w \times t}. \tag{2}$$

2.2 Experimental set-up

The experimental apparatus is shown in Figure 2. Uniaxial tensile experiments are con-

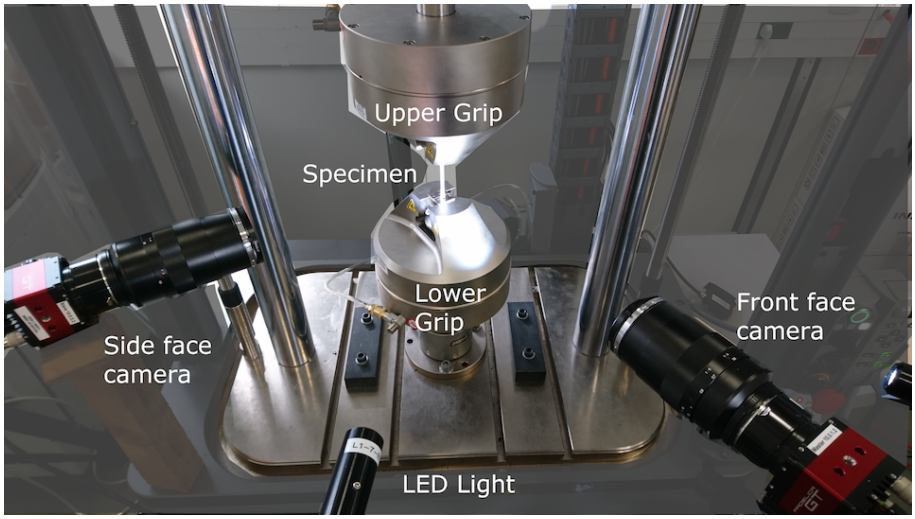

Figure 2: Experimental set-up with camera positioning.

ducted with a Instron ElectroPulse E10000 (linear-torsion all electric-dynamic machine); it is equipped with a 1 kN load cell and high pressure grips. During the experiments, displacement is prescribed at speed 10 mm/min, during the whole cycle (both loading and unloading). For each porosity, the experiments are conducted twice, on different samples. Both displacement and force F are recorded at 20 Hz.

In addition to these global measurements, local surface measurements of strain are carried out. For this purpose, two Prosilica GT6600 29 Mpix cameras (resolution 6576×4384 Pix^2) with 100 mm Zeiss Makro-planar 2/100ZF lenses record the deformation of the sample throughout the test: the front face camera records the deformation of the face normal to the thickness, and the side face camera records the deformation of the face normal to the width (see Fig. 2). Then, Digital Image Correlation (DIC) provides the three stretch ratios of Eq. (1). The method used here is almost similar of the one of Crevoisier et al (2012), with two cameras facing the two sides of the sample. Here, due to large strain no parasitic bending occurs, then the authors assume that the strain field measured on both sides are equal to the strain field on the corresponding opposite hidden faces. Note that a more precise technique would consist in using two sets of two cameras and in performing stereo correlation on two opposite sides of the sample (Wu et al, 2011). From a practical point of view, the gauge length of the specimens is covered with a black paint

Figure 3: Virtual strain gauges on undeformed samples. Top: front face. Bottom: side face.

speckle as shown in Figure 3. Displacement and strain fields are computed thanks to VIC-2D software (Correlated Solutions). Mean values of the logarithmic strain tensor are calculated thanks to a virtual strain gauge (black rectangles in Fig. 3). The dimensions of these gauges are about 15×4.5 mm^2 for the front face (Fig. 3(top)) and 15×1.5 mm^2 for the side face (Fig. 3(bottom)). The corresponding optical and DIC parameters are summarized in Tables 2 and 3, respectively.

Camera	Allied Vision Technology Prosilica GT6600
Dynamic range, image	8 bits
Lens	100 mm Zeiss Makro-planar 2/100ZF
Field of view	110×73 mm^2
Patterning technique	Black spray paint

Table 2: Image acquisition parameters.

DIC Software	VIC-2D version 8.
Subset shape function	6-tap spline
Strain formulation	Logarithmic
Matching Criterion	NSD

Table 3: DIC parameters.

3 Results and discussion

All data investigated here are available in Coret et al (2022). Thus, in the following we sometimes choose to not present the results for all porosities.

3.1 Isotropy

Classically, isotropy of such materials is assumed. Thanks to the two cameras, it is possible to verify this assumption. As examples, Figure 4 presents the comparison of λ_w and λ_t for 0% and 20% filled materials. For all volume fractions (not shown here), results are

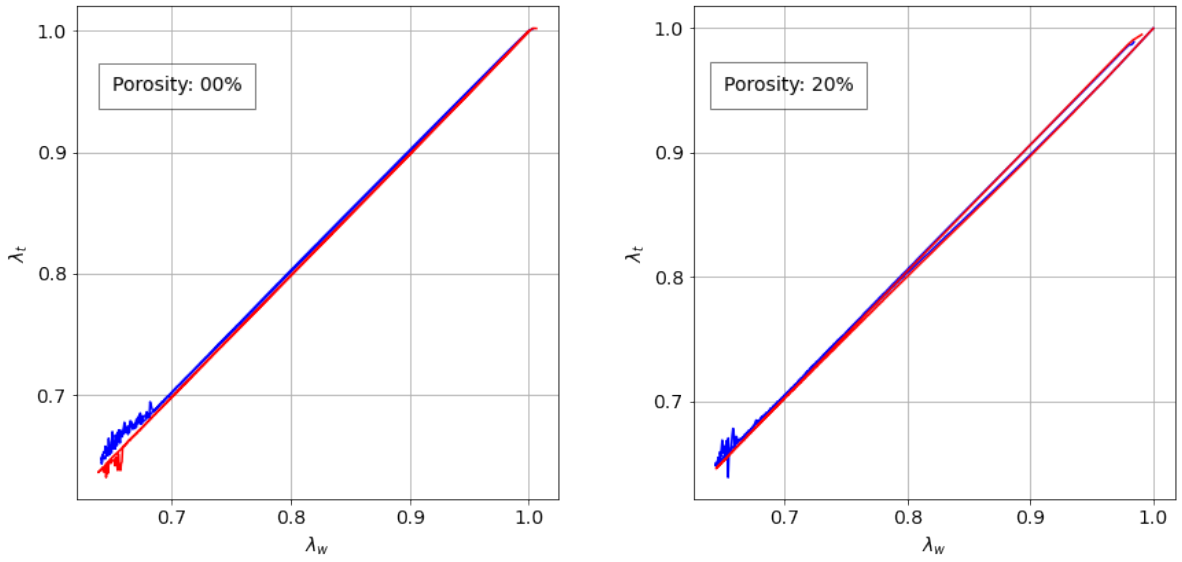

Figure 4: Isotropy of the materials. Porosity: 0% (left), 20% (right). The red and blue lines correspond to two different experiments.

identical: $\lambda_w = \lambda_t$ during all the experiments. *Thus, all materials are isotropic.*

In the following, only λ_w will be considered when necessary. Indeed, its measurement is more precise than the one of λ_t because the analysed surface is larger in the width direction (see Fig. 3).

3.2 Repeatability, averaging and smoothing

As mentioned above, experiments are conducted twice for a given material. In all cases, measurements are repeatable and reproducible. Then a mean curve is calculated for each material. This curve is a bit noisy due to the sampling frequency of the force measurement (20 Hz) and to the low measured values of the loading force as compared to the load cell capacity (1 kN). Then, it is smoothed by a Savitzky-Golay filter with a polynomial of degree 2 (Scipy documentation, 2021). This process is illustrated in Figures 5 and 6 for the 0% and 20% filled materials respectively. Similar results are obtained for the four other materials.

Through the rest of the paper, all analyses will be performed considering smoothed mean curves.

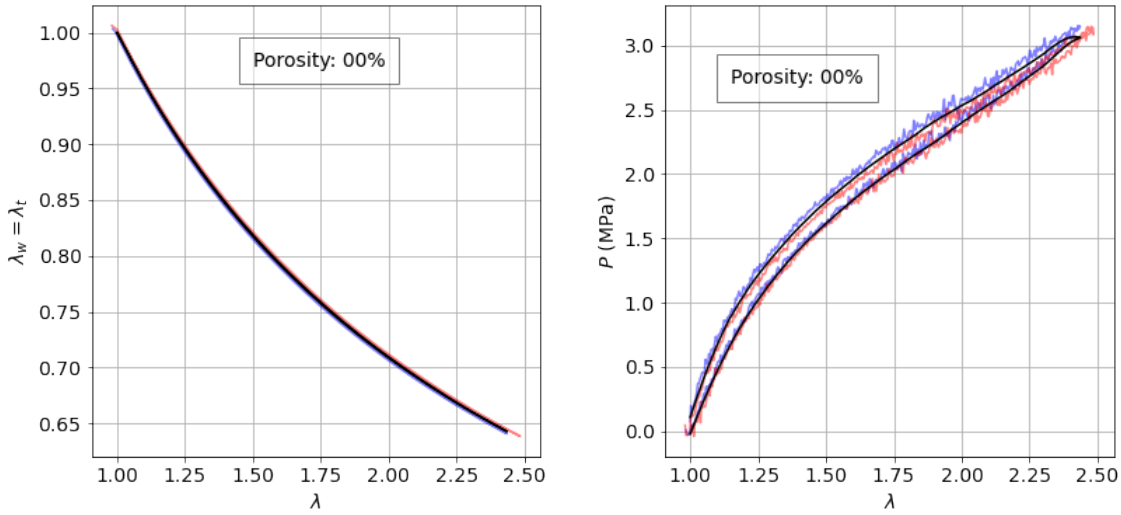

Figure 5: Lateral stretch ratio (left) and nominal stress (right) vs. extension. Porosity: 0%. In blue and red: raw data of the two experiments; in black: the corresponding averaged and smoothed curve.

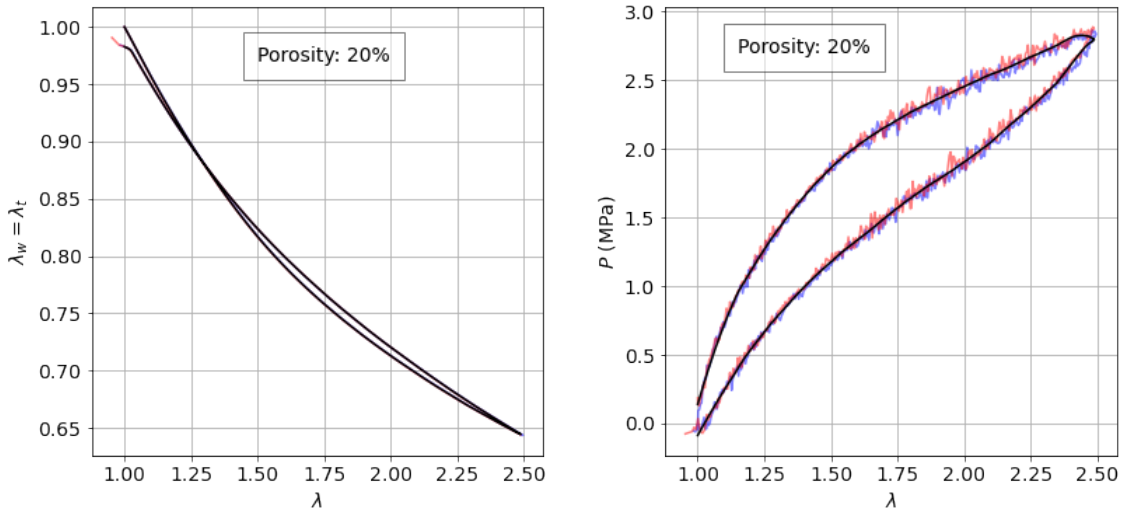

Figure 6: Lateral stretch ratio (left) and nominal stress (right) vs. extension. Porosity: 20%. In blue and red: raw data of the two experiments; in black: the corresponding averaged and smoothed curve

3.3 Classical results in uniaxial tension

Standard results of uniaxial tensile tests are depicted in Figure 7. The left-hand side plot shows the evolution of the transversal stretch ratio ($\lambda_w = \lambda_t$) with respect to the longitudinal one (λ), and the right-hand side plot shows the stress-strain loading-unloading

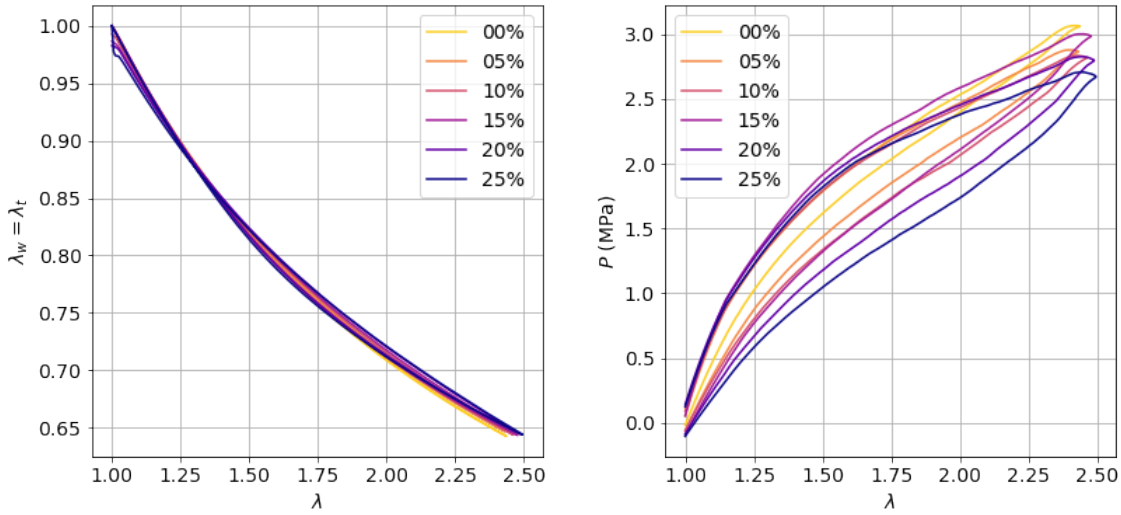

Figure 7: Lateral stretch ratio (left) and nominal stress (right) vs. stretch ratio for all materials.

curves.

From a general point of view, these results are very classical and looks like the ones obtained with pure elastomers: stress-strain curves exhibit the traditional hysteresis loop. Nevertheless, a more precise comparison of the curves leads to the following comments.

- At first sight, the λ_w vs. λ evolution curves are very similar whatever the volume fraction of HTMs. Moreover, the corresponding hysteresis loops between loading and unloading are very small.

- All stress-strain curves admit the same shape and the same initial stiffness. Loading curves exhibit differences in stiffness for $\lambda \simeq 1.6 - 1.7$: the higher the porosity of HTMs, the more the stiffness decreases. An opposite trend has been observed by Shorter et al (2007), but the initial stiffness of the materials were highly different from one to another. Moreover, it is to note that the curve of the 15% material does not follow the general trend: for $\lambda = 2.5$, it is above the 5% and 10% curves.

- All stress-strain curves present a hysteresis loop between loading and unloading: the higher the volume fraction of HTMs, the larger the hysteresis loop. This observation is similar to the one of Yousaf et al (2022) for small strain ($\lambda = 1.25$ and 1.4).

- At $\lambda = 1$ on the unloading curves, there is almost no compressive stress. We can roughly conclude that viscous effect are negligible for small strain rates (about 5.10^{-3} s^{-1} at small strain). This result is in accordance with the one of Yousaf et al (2022) who measure about 5% strain for $\max(\lambda) = 1.25$ and about 7-8% for $\max(\lambda) = 1.4$ at zero-stress on the unloading curves, whatever the fraction of HTMs.

We argue that the viscoelasticity of the composite depends on the viscous properties of the elastomer matrix and not on the HTMs volume properties.

3.4 Compressibility

As stated above, the response of the filled materials seems to be quite close to the one of standard elastomers under uniaxial tensile loading conditions. Nevertheless, it is well-known that the major feature of HTMs-elastomer composites is their volumetric response. Thus, in the following we propose a complete analysis of this feature. This approach resembles to the method proposed in Smith et al (2021) for compressive loading conditions.

First, we consider only kinematic quantities. Both the Poisson ratio ν (generalized to large strain) and the volume ratio J (Jacobian determinant of the deformation gradient tensor) are calculated:

$$\nu = -\frac{\log \lambda_w}{\log \lambda} \quad \text{and} \quad J = \lambda \times \lambda_w \times \lambda_t = \lambda \times \lambda_w^2. \tag{3}$$

The corresponding results are plotted in Figure 8.

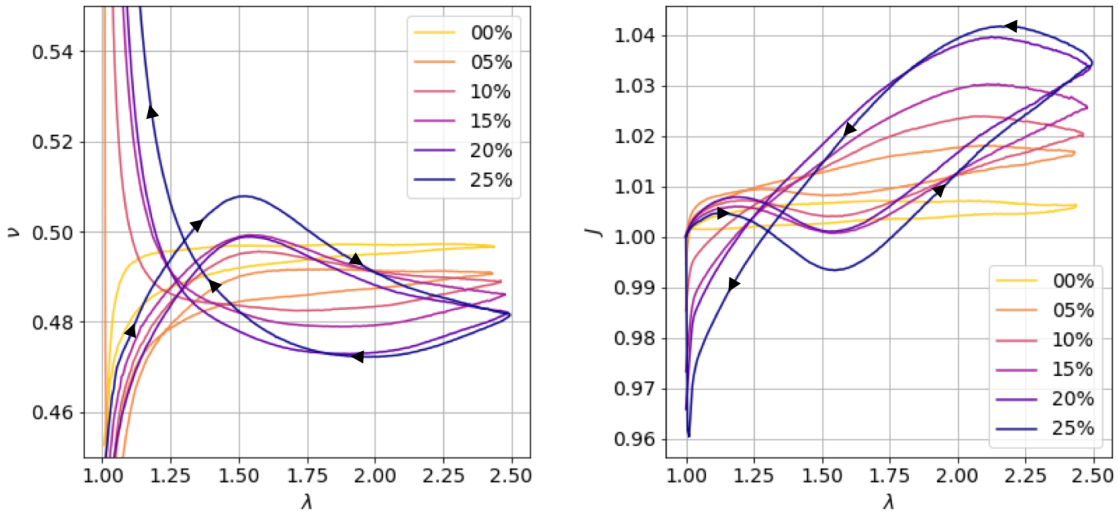

Figure 8: Poisson ratio ν (left) and change in volume J (right) vs. extension. The loading-unloading path is shown by the black arrows.

For both quantities, the curves exhibit hysteresis loops which size increases with the volume fraction of HTMs. It is to note that this response was not predictable by examining the evolution of lateral stretch in Fig. 7(left). As shown in Fig. 8(left), the results for $\lambda < 1.2$ are not relevant (division by $\log \lambda$ with λ near 1). For larger values, ν varies between 0.47 and 0.51. It reveals that the materials are almost incompressible, but the shape of the curves highlight a complex response "around" incompressibility. This complexity becomes obvious when examining the evolution of J depicted in Fig. 8(right). Except the

curve of the pure polyurethane (0%), all curves admit a large hysteresis loop, with several changes of slope during the cycle. It is important to note again that it corresponds to very small changes in volume: between -0.5% to 4% for the material with 25% HTMs.

3.5 Volumetric response

To further investigate this unusual phenomenon, we consider now the stress-strain volumetric response of the materials. In this way, the hydrostatic pressure is calculated. It is defined as

$$p = -\frac{1}{3}\mathrm{tr}\boldsymbol{\sigma}, \tag{4}$$

where $\boldsymbol{\sigma}$ is the Cauchy stress tensor related to the nominal stress tensor $\boldsymbol{P}$ by

$$\boldsymbol{\sigma} = (\det \boldsymbol{F})^{-1}\ \boldsymbol{P}\boldsymbol{F}^{T}, \tag{5}$$

$\boldsymbol{F}$ being the deformation gradient tensor and $\cdot^{T}$ the transposition operator. Recalling that in the principal directions of deformation (length, width and thickness directions of the sample, see Fig. 1) $\boldsymbol{F}$ is the diagonal tensor which contains the stretch ratios, the Cauchy stress in the loading direction reduces to P/λ_w^2 and all other components of $\boldsymbol{\sigma}$ are null. Thus,

$$p = -\frac{1}{3}\frac{P}{\lambda_w^2}. \tag{6}$$

As this pressure is always negative in uniaxial tension (because $P \geq 0$), $-p$ is used to plot the graphs. Nevertheless, we have to keep in mind that the pressure is positive, i.e. it tends to increase the volume of the material.

The corresponding volumetric responses J vs. $-p$ are presented in Figure 9. First,

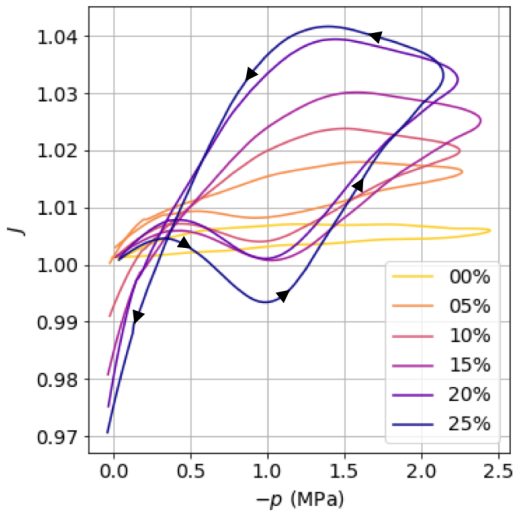

Figure 9: Volumetric response of the six materials.

the curve of the virgin material (0%) is classical for a quasi-incompressible elastomer: it presents a small hysteresis and for a change in volume of about 0.5% ($J = 1.005$), the pressure increases sharply with the volume change. Second, all the other curves have the same complex shape: they present a hysteresis loop that increases with the HTMs volume fraction. Moreover, they exhibit a non-monotonous form with several extrema.

In order to investigate the features of these hysteresis loops, some descriptive notations are introduced. Consider the schematic hysteresis loop depicted in Figure 10. During a

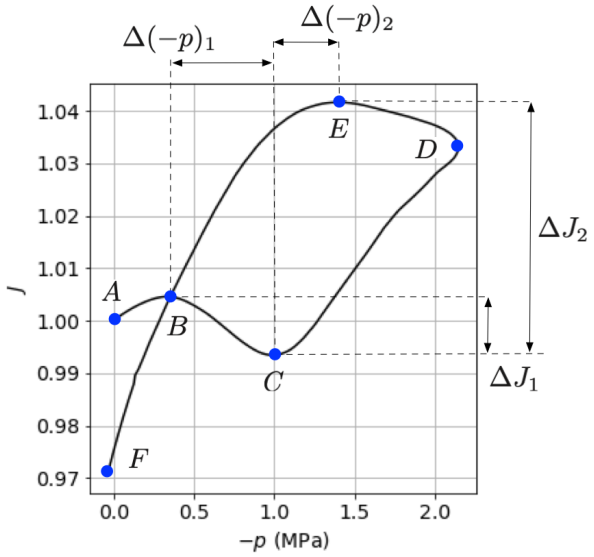

Figure 10: Description of the volumetric response. Definition of the extrema and the jumps, example of the 25% filled material.

loading-unloading cycle, the loop passes through points A to F defined by the blue circles in the figure. Once again, arrows depict the loading-unloading path. Points are defined as follow:

A. Departure point: $J = 1$ and $-p \approx 0$. Then the volume increases until point B.

B. First maximum point. Then the volume decreases until point C.

C. The minimum of the loading part. It is to note in Fig. 9 that for 15% and 20%, $J \simeq 1$ (it went back to the undeformed volume) for $-p \simeq 1$ MPa. For 25%, the volume has diminished for the same pressure.

D. It is the maximum loading point, it corresponds to $\lambda \simeq 2.5$ and to the maximum pressure borne by the material. The unloading begins and the volume continue to increase until point E.

E. This is the maximum change in volume attained during the cycle. After this point, the volume decreases through the rest of the unloading path.

F. It is the end of the cycle; at this point $\lambda = 1$. There is a remanent change in volume. With our results, it is difficult to know if it is irreversible (damage) or if the sample will recover its initial dimensions (viscous effect).

To continue the discussion, four additional quantities are introduced: the pressure jumps

$$\Delta(-p)_1 = -\left(p(C) - p(B)\right) \quad \text{and} \quad \Delta(-p)_2 = -\left(p(E) - p(C)\right) \tag{7}$$

and the volume change jumps

$$\Delta J_1 = J(C) - J(B) \quad \text{and} \quad \Delta J_2 = J(E) - J(C), \tag{8}$$

as shown in Fig. 10.

First, Figure 11(left) shows the maximum of the hysteresis loops (points B, C, and E) for the five filled materials. Second, Fig. 11(right) presents the corresponding jumps couples $(\Delta(-p), \Delta J)$. In Fig. 11(left), we verify the previous observation: the larger

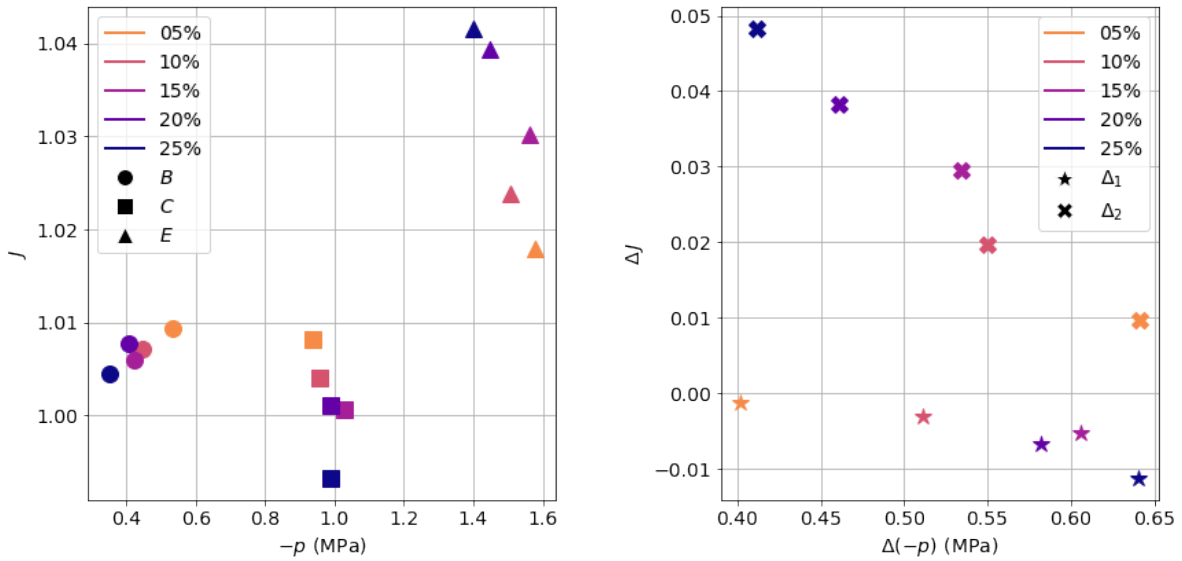

Figure 11: Analysis of volumetric curves. Left: extrema; Right: jumps.

the HTMs volume fraction, the bigger the hysteresis loop. Indeed, extreme values of the change in volume J increase with the HTMs porosity for the maxima (point E) and decrease with it for the minima (point C). Nevertheless, it is interesting to mention that these extrema take place for almost the same pressure whatever the material: about 0.4 MPa for point B, 1 MPa for point C and around 1.5 MPa for point E. Similar conclusions can be drawn thanks to Fig. 11(right). For the jump in volume change, it is obvious: the larger the HTMs volume fraction, the larger the second jump ΔJ_2 and the smaller (negative) the first one ΔJ_1. For the pressure jump, it is more complicated, because the second jump $\Delta(-p)_2$ decreases as the volume fraction increases.

Finally, to close this presentation of the results, the volume and pressure jumps are plotted with respect to the porosity in Figure 12. Examining Fig. 12(left) leads to a

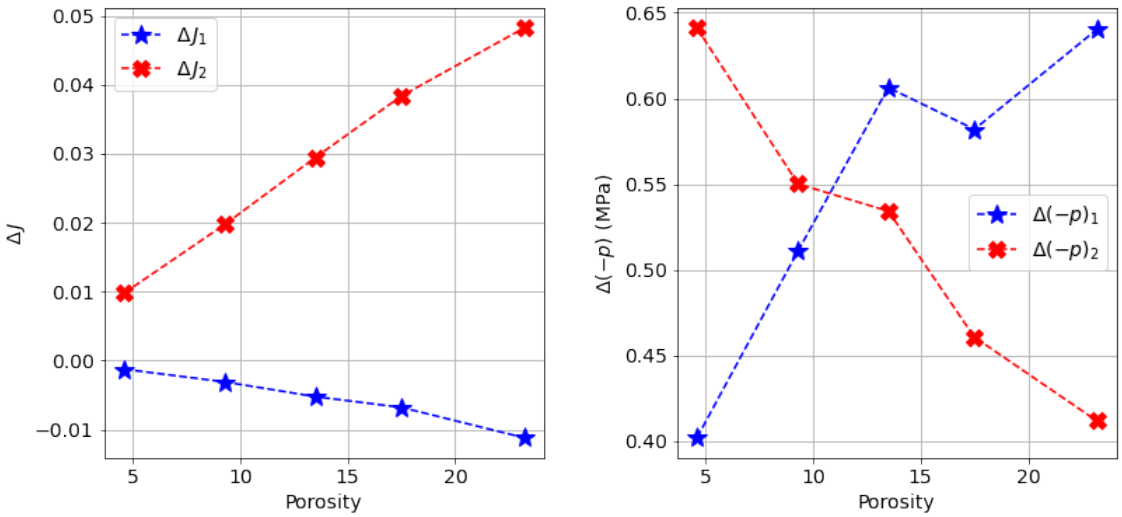

Figure 12: Jumps vs. porosity. Left: volume change; right: hydrostatic pressure.

surprising observation: both volume change jumps evolve linearly with the HTMs volume fraction. For pressure, it is not exactly similar: the data corresponding to 15% are not exactly aligned with other points (see Fig. 12(right)). It is related to the previous observation of Fig. 7(right) in which the 15% stress-strain curve is above the 5% and 10% ones. In our opinion, this discrepancy may be due to defects in the 15% material (even if the two tests were almost superimposed); but it does not mitigate the remarkable characteristics of the phenomena highlighted in the present paper.

4 Conclusion

In this paper, a thorough analysis of uniaxial tensile experiments on polyurethane elastomer filled with hollow thermoplastics spheres has been conducted. Thanks to a two-camera setup and digital image correlation, the surprising volumetric response of such materials has been exhibited. Even if the lateral stretch and nominal stress vs. loading stretch curves are very classical and look like the ones of standard elastomers, the change in volume vs. pressure curve exhibits several slope changes in the loading-unloading hysteresis loop.

This remarkable macroscopic response is the signature of complex microstructural phenomena; as emphasized by Yousaf et al (2022) in the case of uniaxial extension it might be explained by the "debonding of microspheres from the matrix material". Such possible explanations necessitate further investigation, and we hope that the present observations will help to understand and model the mechanical response of HTMs filled elastomers.

References

Brown JA, Carroll JD, Huddleston B, et al (2018) A multiscale study of damage in elastomeric syntactic foams. Journal of Materials Science 53(14):10,479–10,498. https://doi.org/https://doi.org/10.1007/s10853-018-2263-y

Coret M, Verron E, Rublon P (2022) Images and data accompanying article: Remarkable response of hollow thermoplastic microspheres-elastomer matrix composites in uniaxial tension. [data set]. Zenodo https://doi.org/https://doi.org/10.5281/zenodo.6390478

Crevoisier JD, Besnard G, Merckel Y, et al (2012) Volume changes in a filled elastomer studied via digital image correlation. Polymer Testing 31(5):663–670. https://doi.org/https://doi.org/10.1016/j.polymertesting.2012.04.003

Curd ME, Morrison NF, Smith MJA, et al (2021) Geometrical and mechanical characterisation of hollow thermoplastic microspheres for syntactic foam applications. Composites Part B: Engineering 223:108,952. https://doi.org/https://doi.org/10.1016/j.compositesb.2021.108952

De Pascalis R, Abrahams ID, Parnell WJ (2013) Predicting the pressure–volume curve of an elastic microsphere composite. Journal of the Mechanics and Physics of Solids 61(4):1106–1123. https://doi.org/https://doi.org/10.1016/j.jmps.2012.11.005

Gupta N, Ye R, Porfiri M (2010) Comparison of tensile and compressive characteristics of vinyl ester/glass microballoon syntactic foams. Composites Part B: Engineering 41(3):236–245. https://doi.org/https://doi.org/10.1016/j.compositesb.2009.07.004

Gupta N, Zeltmann SE, Shunmugasamy VC, et al (2014) Applications of polymer matrix syntactic foams. JOM, The Journal of Minerals, Metals & Materials Society 66(2):245–254. https://doi.org/https://doi.org/10.1007/s11837-013-0796-8

Paget B, Zinet M, Cassagnau P (2021) Syntactic foam under compressive stress: Comparison of modeling predictions and experimental measurements. Journal of Cellular Plastics 57(3):329–346. https://doi.org/https://doi.org/10.1177/0021955X20943112

Scipy documentation (2021) https://docs.scipy.org/doc/scipy/reference/generated/scipy.signal.savgol_filter.html. Version 171

Shorter R (2014) The mechanical behaviour of elastomers when hollow microspheres are used as a particulate filler. PhD thesis, Queen Mary University of London

Shorter R, Thomas AG, Busfield JJC, et al (2007) The physical behaviour of elastomers containing hollow spherical fillers. In: Boukamel A, Laiarinandrasana L, Méo S, et al (eds) Constitutive Models for Rubber V: Proceedings of the 5th European Conference. CRC Press

Shrimali B, Parnell WJ, Lopez-Pamies O (2020) A simple explicit model constructed from a homogenization solution for the large-strain mechanical response of elastomeric syntactic foams. International Journal of Non-Linear Mechanics 126:103,548. https://doi.org/https://doi.org/10.1016/j.ijnonlinmec.2020.103548

Smith MJA, Yousaf Z, Potluri P, et al (2021) Modelling hollow thermoplastic syntactic foams under high-strain compressive loading. Composites Science and Technology 213:108,882. https://doi.org/https://doi.org/10.1016/j.compscitech.2021.108882

Wu T, Coret M, Combescure A (2011) Strain localisation and damage measurement by full 3d digital image correlation: application to 15-5ph stainless steel. Strain 47(1):49–61. https://doi.org/https://doi.org/10.1111/j.1475-1305.2008.00600.x

Yousaf Z, Smith M, Potluri P, et al (2020) Compression properties of polymeric syntactic foam composites under cyclic loading. Composites Part B: Engineering 186:107,764. https://doi.org/https://doi.org/10.1016/j.compositesb.2020.107764

Yousaf Z, Morrison N, Parnell WJ (2022) Tensile properties of all-polymeric syntactic foam composites: experimental characterization and mathematical modelling. Composites Part B: Engineering 231:109,556. https://doi.org/https://doi.org/10.1016/j.compositesb.2021.109556